Materials Today Electronics 3 (2023) 100029

Contents lists available at ScienceDirect

Materials Today Electronics

journal homepage: www.elsevier.com/locate/mtelec

Full Length Article

The structural, optical and electrical properties of sodium titanate nanotubes sensitized with nitrogen/sulfur co-doped graphene quantum dots as potential materials for quantum dots sensitized solar cells

Martin Esteves[a,b], Dominique Mombrú[a], Mariano Romero[a], Luciana Fernández-Werner[a,*], Ricardo Faccio[a,*], Alvaro W. Mombrú[a,*]

[a] Centro NanoMat/CryssMat-Lab & Grupo Física, DETEMA, Facultad de Química-Universidad de la República (UdelaR), Montevideo CP 11800, Uruguay
[b] Graduate Program in Chemistry, Facultad de Química, Universidad de la República, Av. Gral. Flores 2124, CC 1157, CP 11800 Montevideo, Uruguay

A B S T R A C T

In this work, we present the synthesis of nanoscale heterostructures of sodium titanate nanotubes $Na_2Ti_2O_5.H_2O$ (NaNT) decorated with N- and S- co-doped graphene quantum dots (NS-GQD) for quantum dots sensitized solar cells (QDSSC). The study was mainly focused on the structural, microstructural, electrical and optical characterization of these nanoscale heterostructures by means of X ray diffraction, transmission electron microscopy, atomic force microscopy, Raman, UV–vis and impedance spectroscopies. Our nanoscale heterostructures yielded a significant enhancement in the electric conductivity interpreted in terms of favorable interactions between the NS-GQD and the NaNT acting as proper connectors. Finally, our QDSSC prototype exhibits promising values for diffusion coefficient and recombination times as evidenced by means of impedance modulated photocurrent and photovoltage spectroscopies. Also, we consider that these materials could be further explored for electron transport layers applications in order to exploit the advantages regarding electron transport properties.

1. Introduction

Titanium oxide is one of the most commonly used semiconductors for solar cell and photocatalytic applications due to its chemical stability, low cost, non-toxicity, and wide availability [1,2]. In addition to these properties, titanium oxide has a proper electronic structure characterized by dissimilar orbitals conforming to the valence and conduction band which helps to prevent electron recombination [3]. Different polymorphs, considering various sizes, morphologies and aspect ratios have been studied [4–8]. In particular, the tubular structures are interesting because of the enchantment of one-directional electronic mobility and the decreasing of interparticle contacts, providing better electronic transport [4]. These structures are characterized by layered structures with the capability of interchanging ions in between the layers [9]. They also present a high superficial area and have shown interesting properties for semiconductor devices, and photovoltaics applications [10], among others. However, TiO_2 and its titanates derivates structures have a major drawback; they present such a big band gap that can only be activated under UV irradiation. For this reason, it is necessary to use some sensitizer agent that could be triggered by visible light in order to have better use of the incident solar radiation [11,12]. Generally, synthetic dye based on ruthenium polypyridyl complexes have proved to be very efficient sensitizers. However, due to the utilization of heavy metal the cost production is found to be expensive and also unstable under long term use [13,14]. One recent strategy consists of preparing carbon-titanium composite materials in order to improve the solar cell efficiency [15]. The most usual carbon materials used in these composites are carbon nanotubes, graphene and graphene quantum dots (GQD) [16–19]. Among these carbon nanostructures GQDs have discrete electronic levels, allowing hot electron injection, efficient charge separation and the possibility to tune their band gap by quantum confinement effects and edge effects. Also, the π extended system could interact with the TiO_2 surface [19]. Among the different modifications that can be made to GQD in order to achieve better sensitization properties, the doping with nitrogen (N), which has a comparable atomic size compared to carbon (C) and has five valence electrons, is one of the most interesting ones yielding to a reduction in the electronic band gap and hence taking a better use of the incident radiation [20]. Also, nitrogen (N) and sulfur (S) co-doping has been tested in NS-GQDs yielding to even lower energy band gaps that can be triggered by visible light. The presence of S atoms is reported to enhance the electronic transfer process towards the TiO_2 surface and minimize charge recombination in DSSC [20,21]. In this context, we present a facile way of preparing NS-GQDs co-doped $Na_2Ti_2O_5.H_2O$ titanate nanotubes using the Kasuga method [22], showing considerable improvements in the electrical conductivity and a strong sensibilization in the visible region.

* Corresponding authors.
E-mail addresses: lucianaf@fq.edu.uy (L. Fernández-Werner), rfaccio@fq.edu.uy (R. Faccio), amombru@fq.edu.uy (A.W. Mombrú).

https://doi.org/10.1016/j.mtelec.2023.100029
Received 16 December 2022; Received in revised form 4 March 2023; Accepted 14 March 2023
Available online 21 March 2023

2. Methods

2.1. Synthesis of sodium titanate nanotubes (NaNT)

Sodium titanate nanotubes ($Na_2Ti_2O_5{\cdot}H_2O$), labeled as NaNT, were prepared by an alkali hydrothermal method. 1.25 g of TiO_2 anatase purchased from Sigma-Aldrich were dispersed on 75 mL of NaOH solution (10 mol/L); the reactor fill factor was set to 2/3, kept stirred at 120 rpm and heated to 145 ˚C for 24 hs. The resulting suspension was washed several times with distilled water in order to remove the NaOH excess. The obtained solid was finally dried overnight at 70 ˚C [23].

2.2. Synthesis of NS co-doped graphene quantum dots (NS-GQD)

Nitrogen/sulfur co-doped graphene quantum dots were prepared following Qu *et al.* synthesis [24]. In summary, NS-GQD was prepared by mixing 1.05 g of citric acid and 1.15 g of thiourea in 25 ml of distilled water. The solution was transferred into a 100 ml Teflon-lined stainless-steel autoclave at 120 rpm and 160 ˚C during 18 h. The final product was washed by adding ethanol and water and centrifuged several times.

2.3. Synthesis of NaNT:NS-GQD system

An approximate amount of 200 mg of NaNT was suspended in 20 mL of ethanol followed by the dropwise addition of NS-GQDs suspensions. The NaNT:NS-GQD mixture was vigorously stirred overnight until dryness. Different NS GQDs weight fraction composites were prepared: 1%, 5% and 15% w/w, named as NaNT:NS-GQD-X, with X = 1%, 5% and 15%, respectively.

2.4. Quantum dots sensitized solar cells (QDSSc) prototype assembling

Photoelectrodes were made of two layers of semiconductor materials. The first layer consists of a compact layer of anatase nanoparticles deposited onto the FTO conductive glass by Doctor Blade [25] technique using the commercially available dye sol® TiO_2 paste. This layer was sintered at 400 ˚C for 3 h. The second layer was applied using the same method but deposited onto the TiO_2 first layer. In this case, a paste of NaNT:NS-GQD composite using a few drops of diluted acetic acid and ethylene glycol was prepared and deposited by Doctor Blade technique. The film was dried at 150 ˚C for 2 h. A few extra drops of NS-GQD were added as extra sensitizer and let it sensibilize for 24 h. The counter electrode was screen printed with Pt on a FTO substrate using Platinum paste screen printable Aldrich and heating on a muffle at 450 ˚C overnight.

2.5. Characterizations

NS-GQDs, NaNT and NaNT:NS-GQDs composites systems were studied by X-ray powder diffraction, using a Rigaku Ultima IV diffractometer, working in Bragg-Brentano configuration under CuKα radiation with 0.02˚ steps in the 2θ range 5.00˚–80.00˚. The size and morphology of NaNT:NS-GQDs samples were studied using a JEOL JEM 1010 with an acceleration voltage of 100 kV. Sample was dispersed in ethanol and dropped onto a carbon film supported by a copper grid. Raman spectra for all samples were collected using WITec Alpha 300-RA equipment, working with an excitation laser wavelength of 532 nm. All these procedures are in agreement with a previous methodology [23,26,27]. Atomic force microscopy (AFM) in the AC mode for graphene quantum dots dried onto silicon wafers was performed using the same equipment, utilizing a silicon cantilever of 42 N/m operating at 270 kHz frequency. Solid state reflectance measurements were carried on a UV–vis spectrophotometer Shimadzu UV-2600i with an integrating sphere in the 700 –300 nm range [26,27]. The AC impedance spectroscopy analysis was performed using a Gamry Reference 3000 impedance analyzer at T ~ 300 K using an AC voltage amplitude of 300 mV in the frequency range of 1 Hz – 1 MHz. Additional AC impedance spectroscopy analyses were performed on a QDSSC prototype under the same conditions but using AM 1.5 conditions at an applied cells V_{oc}.

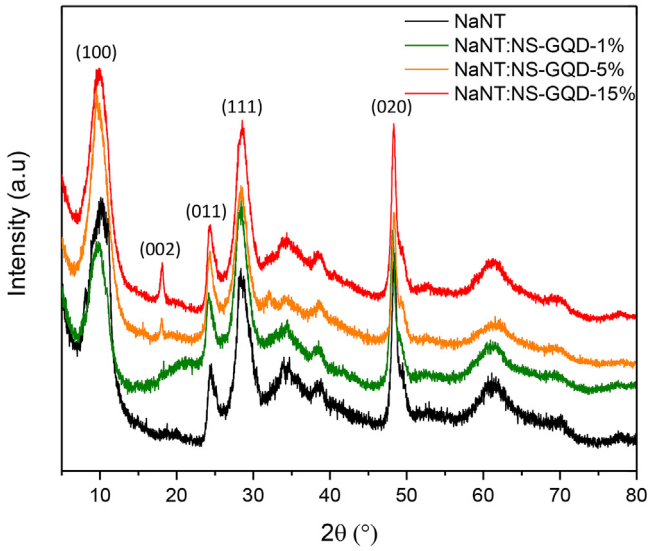

Fig. 1. XRD for NaNT, NaNT:NS-GQD 1%, NaNT:NS-GQD 5% and NaNT:NS-GQD 15%.

3. Results and discussion

3.1. Structural and morphological characterization

X-ray diffraction patterns (XRD) for $Na_2Ti_2O_5.H_2O$ nanotubes (NaNT) and the composites NaNT:NSGQD 1%, NaNT:NS-GQD 5% and NaNT:NSGQD 15% are shown in Fig. 1. The main signals on the pattern located at ~9.2˚, 24.0˚, 28.6˚ and 48.3˚ can be assigned to (100), (011), (111) and (020) Bragg planes of NaNT, as already studied in our previous report. [23] The broadest peak at ~9.2˚ confirms that the radial direction of the tubes is according to the crystallographic *a*-axis. The correlation distance associated with this signal is about 9.8 Å, which corresponds to the space between [TiO_5] layers. It is possible to estimate a wall thickness of about 3.4 nm by applying the Scherrer equation on this particular Bragg reflection. The narrowest signal indicates the major coherence direction, suggesting that the axial direction of the tube is according to *b*-axis. It is possible to estimate a 16 nm mean crystalline size domain using the Scherrer equation. One interesting feature is the increase in the intensity of a peak located at ~ 18.0˚ as long as the amount of NS-GQD is higher. This signal can be ascribed to (002) of the sodium titanate nanotubes' Bragg planes. It is important to remark that the *c*-axis correspond to the tangential direction of the nanotubes, *i.e.* the lowest coherence direction. Thus, the increase in the intensity of this peak can be ascribed to a sort of exfoliation mechanism induced by the NS-GQDs acting as a surfactant, intercalating in the space between layers. Furthermore, the calculated coherence distance for this signal is about 24 nm which is reasonable for partially unwrapped nanosheets since this distance value is upper bounded for the maximum possible unwrapping value of $2\pi R \sim 40\ nm$. Another feature to take into account is the shift towards lower 2θ in the (100) signal as the amount of NS-GQD increases. This could be understood in terms of the increase in the interlaminar titanate planes distance as a result of the loss of internal tensions due to the tubular morphology and the further relaxation when unwrapping.

This unwrapping of the tube could explain the major coherence due to the increasing induced planarity of TiO_2 layers in c-direction when increasing the amount of NS-GQDs. TEM images, shown in Fig. 2, present the comparison between NaNT nanotubes and NaNT:NS-GQD 15% nanocomposite. No significant changes in the tubes' morphology

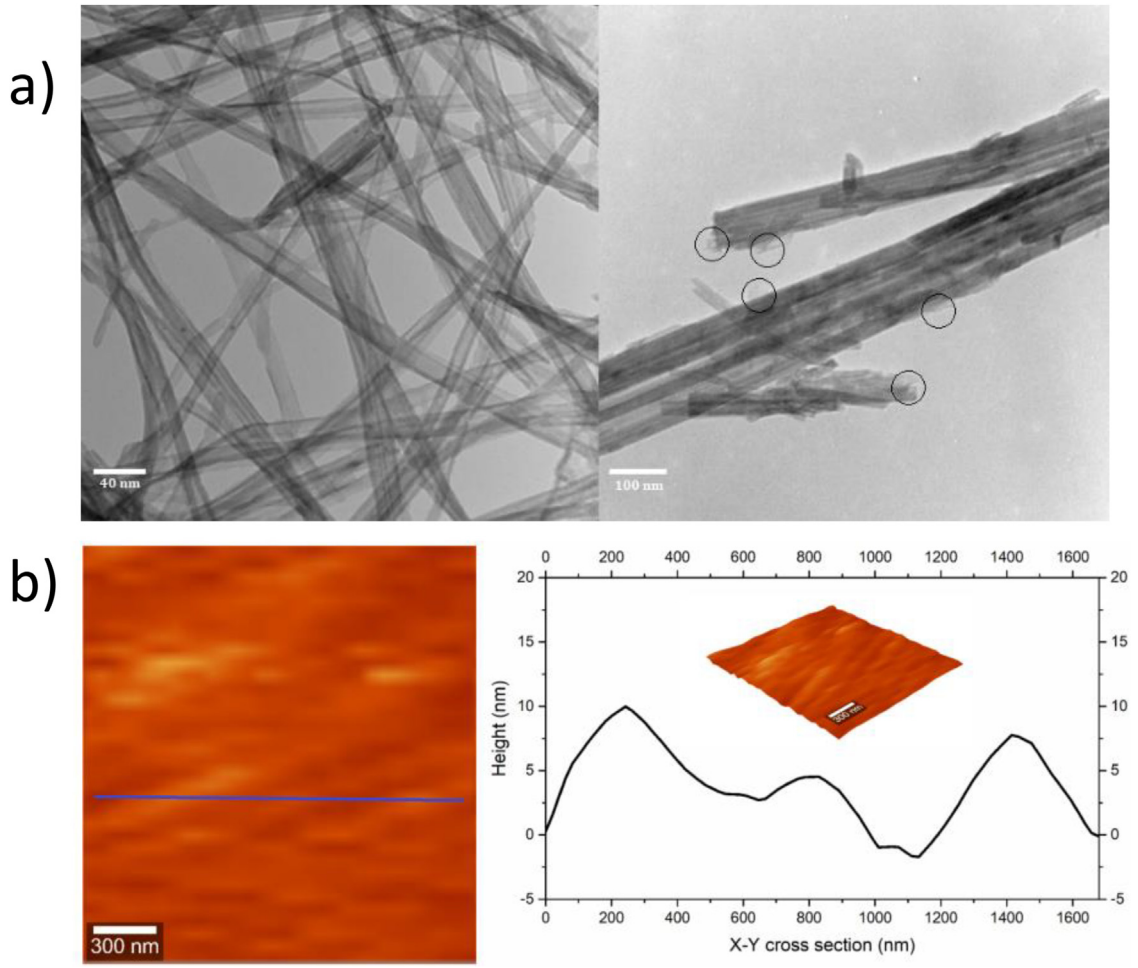

Fig. 2. **a)** TEM pictures of crystalline NaNT (left) and NaNT:NS-GQD 15% (right) (upper panel). B) AFM images with corresponding cross section for NS-GQD (lower panel).

could be detected. However, some sort of texturization, changes in the aggrupation of the tubes, and partial exfoliation in their extremes are seen in NaNT:NS-GQD 15% sample, these features are consistent with the hypothesis of strong interaction between NaNT and NaNT:NS-GQD which can lead to a partial exfoliation of the tubes. AFM image and selected height cross-section for NS-GQD dried solution are shown in Fig. 2**b**. The presence of clusters of few-layered GQDs was observed. Raman spectrum for NS-GQD is shown in Fig. 3**a**, and exhibits peaks at ~ 1350 and 1580 cm^{-1}, associated with the D and G modes of GQDs, respectively, as typically observed in the literature [24,28,29].

Fig. 3**b** presents the low-frequency region of Raman spectra for NaNT and NaNT:NS-GQD composites characterized by the presence of five main bands located at 170, 270, 440, 700 and 900 cm^{-1}. The first four signals can be associated with the Ti–O–Ti vibrational modes in the [TiO_5] layer, and those above 700 cm^{-1} are mainly attributed to the terminal Ti-O stretching mode which is reported to be sensitive to the presence of adsorbed charged species [30,31]. Raman spectra calculations of the bulk titanate were performed in a previous work [23] but due to the low symmetry of this titanate crystal and the presence of structural water molecules, it is not possible to assign the vibration modes to the corresponding irreducible representation. When the amounts of NS-GQD are increased, the Raman peak at 900 cm^{-1} decreases until it disappears. Also, significant shifts are seen in the region 700 cm^{-1}, 440 cm^{-1} and 170 cm^{-1} towards lower Raman shifts as the amounts of NS-GQD increase. The extinction of the 900 cm^{-1} modes can be related to the strong interaction between the terminal Ti-O and the NS-GQD. It is interesting to note that the Raman features obtained with increasing NS-GQD content agree well with the partial un-scrolling and restacking of titanate nanotubes as already observed by Gao et al. [32]. Fig. 3**c** presents the mid-frequency region of Raman spectra for NaNT and NaNT:NS-GQD composites characterized by the presence of the typical D and G modes ascribed to graphene quantum dots for the composites and the expected absence of any signal for NaNT.

3.2. Optical properties of NaNT:NS-GQD systems

Diffuse reflectance measurements were performed on the different composites. The absorption coefficient was calculated according to Kubelka-Munk relationship [33] (Fig. 4**a**) and the corresponding Tauc plots were obtained both considering an indirect (Fig. 4**b**) and direct (Fig. 4**c**) behavior, respectively. It is important to mention that the absorptivity was corrected by removing the background signal. Fig. 4**a** presents the absorption coefficient for NaNT and the NaNT:NS-GQD composites. It is worth noticing that the absorption edge becomes less steep as the amount of NS-GQD increases which could be interpreted qualitatively as an increase in the local disorder in the titanate structure induced by the presence of the NS-GQD. Also, an apparent red shift in the border is observed suggesting an important interaction between NaNT and NS-GQD. When analyzing the indirect band gap behavior, it is possible to see two different absorption borders. The lower energy one can be ascribed to the absorption of the NS-GQD at 1.8 eV and the second one can be ascribed to the indirect gap corresponding to NaNT, which slightly varies from 3.26 eV to 3.16 eV for NaNT-NSGQD-15. Direct band gap measurements show only one border that oscillates from

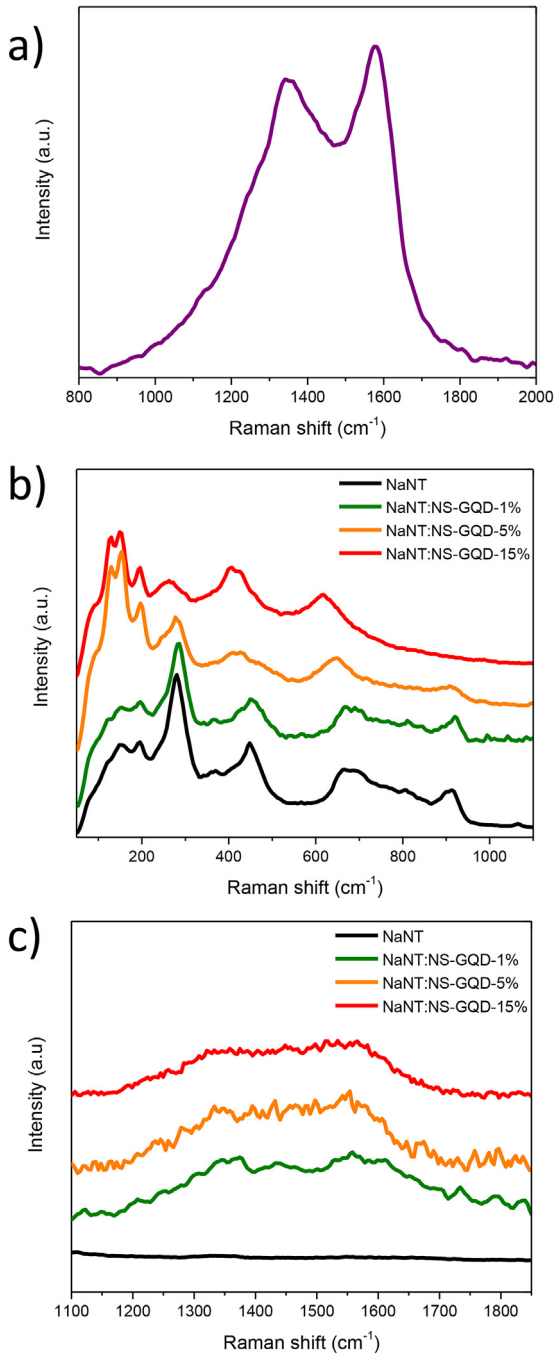

Fig. 3. a) Raman spectra for NS-GQD, b) Raman spectra at 50–1100 cm^{-1} and c) 1100–1900 cm^{-1} for NaNT, NaNT:NS-GQD 1%, NaNT:NS-GQD 5% and NaNT:NS-GQD 15%.

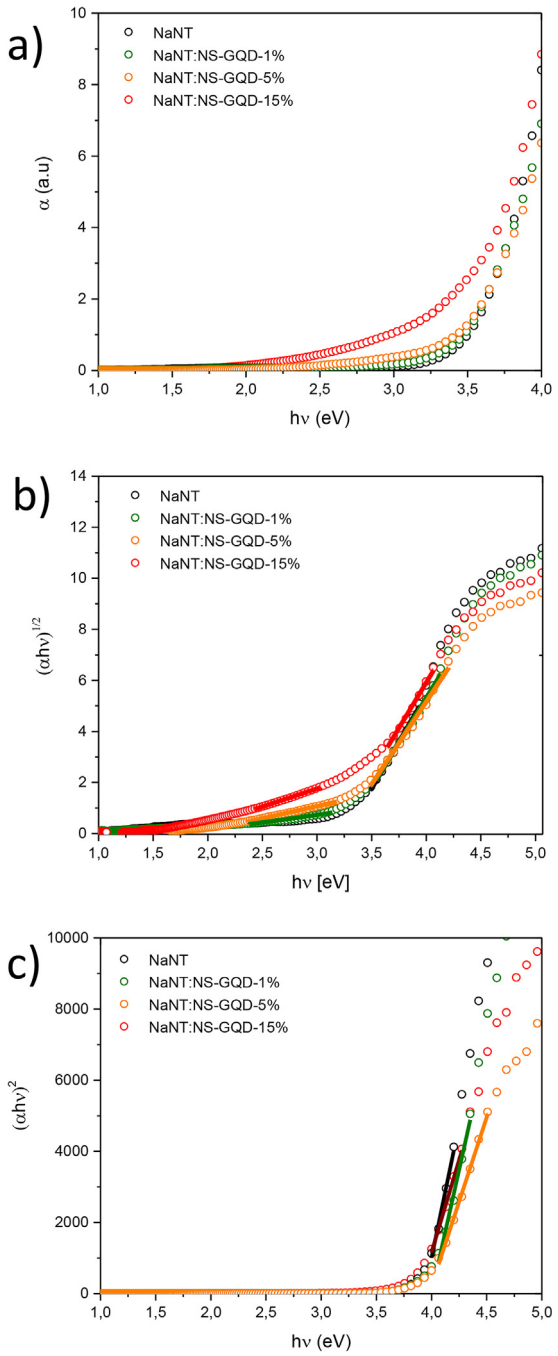

Fig. 4. a) Absorptivity, b) indirect Tauc plot and c) direct Tauc plot (lower panel) for NaNT, NaNT:NS-GQD −1%, NaNT:NS-GQD −5%, NaNT:NS-GQD −15%.

3.88 eV and 3.98 eV. Table 1 summarizes the calculated band gaps. The red shift observed in the absorption borders is ascribed to the appearance of disorder in the titanate structure and consequent impurity levels apparition in the gap rather to a modification of the position of the border.

3.3. Impedance spectroscopy of NaNT:NS-GQD systems

Fig. 5 presents the Nyquist plot for the NaNT and NaNT:NS-GQD composites measured under dark conditions to evaluate the electrical properties of the material previous to the assembling of the solar cell. It is possible to see that as long as the amount of NS-GQD increases the

Table 1
Summary of the calculated energy band gaps.

	E_{g1} Indirect gap (eV)	E_{g2} Indirect gap (eV)	E_g direct gap (eV)
NaNT	–	3.26	3.93
NaNT-NSGQD-1	1.78	3.24	3.88
NaNT-NSGQD-5	1.89	3.20	3.99
NaNT-NSGQD-15	1.76	3.16	3.98

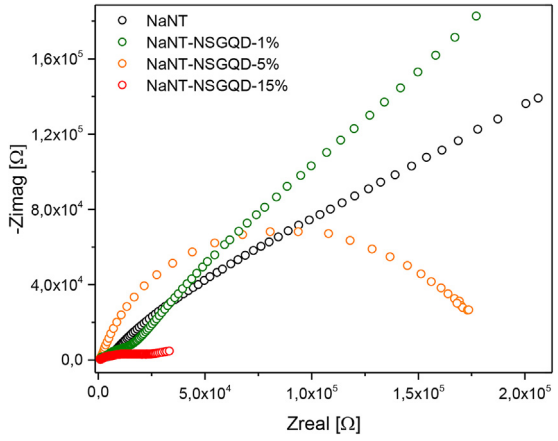

Fig. 5. Nyquist plot for NaNT and NaNT:NS-GQD composites.

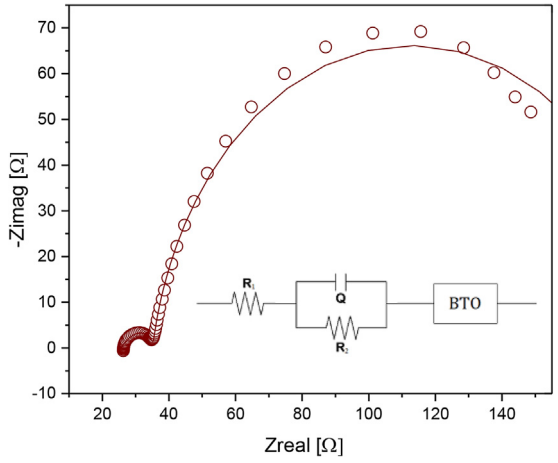

Fig. 6. QDSSC Nyquist plot (scatter) and BTOs equivalent circuit fitting (straight line).

Table 2
Most relevant fitting parameters for the equivalent circuit model used to model the QDSSC by impedance spectroscopy analysis.

R_1 (Ω)	R_2 (Ω)	R_k (Ω)	R_w (Ω)	k_{eff} (s^{-1})
26.7	5.80	152	10.0	1.0

bulk resistance of the composite dramatically decreases. This fact could be ascribed to the interaction between the NS-GQD and the titanate nanotubes yielding to an improvement in the conduction pathway and, thus, to the enhancement of the charge carrier conductivity, consistent with the previous characterizations.

3.4. QDSSC characterization

A prototype of QDSSC was prepared using NaNT-NSGQD-15% as a porous layer. The short circuit current density (J_{sc}) and open-circuit voltage (V_{oc}) yielded J_{sc}=55μA/cm^2 and V_{oc}=0.44 V, respectively. The fill factor is about 0.35 and PCE is below 0.1%. To judge from the previous values, the performance of the cell is quite poor, probably due electron transfer issues between the sensitizer and the semiconductor. For this reason we decided to get better insights of the transport properties in terms of the Bisquert open circuit model [34].

Fig. 6 presents the Nyquist plot for the QDSSC and the most relevant fitting parameters are depicted in Table 2. The origin shift of the first semicircle arc is ascribed to R_1 which represents the resistance due to the contacts and it is about 27 Ω. The high-frequency small semicircle arc

Table 3
Relevant parameters for the QDSSC by IMPS/IMVS spectroscopies.

	τ_{rec} (s)	τ_{trans} (s)	η_{cc}	D_{eff} (cm^2/s)
35 mW/cm^2	1.07	0.277	0.74	5.7×10^{-4}
26 mW/cm^2	1.37	0.377	0.73	6.5×10^{-4}
20 mW/cm^2	1.81	0.475	0.74	5.8×10^{-4}

is ascribed to the Pt electrode interface with a characteristic resistance of 6 Ω [34]. The main semicircle arc is ascribed to the BTO transmission line. The maximum of the semicircle arc is obtained at a frequency of 0.158 Hz which represents a characteristic recombination velocity constant time of 1.0 s^{-1}, which is very high for similar dye sensitized solar cells based on nanostructured TiO_2 as active semiconductor in the photoanode and sensitized with N719 dye [34,35]. However, it is worth noticing that this is also consistent with a relatively low carrier injection regime. Another important parameter is the characteristic relation $R_k/R_w \approx 15$ in the BTO transmission line. Rk represents the resistance associated to the electron transport across the electrolyte/semiconductor interface, and hence also gives information about the recombination process and Rw is the resistance associated to the transport along the semiconductor material [34]. This ratio can be used to estimate the effective diffusion coefficient D_{eff} according to the following relationship (Eq. (1)):

$$D_{eff} = \frac{R_k}{R_w} L^2 k_{eff} \tag{1}$$

where L represents the thickness of the layer and it is roughly estimated to be 120 μm according to the separator used to build the photoanode, yielding $D_{eff} \approx 2.2 \times 10^{-3}$ cm^2/s, which is again a high value consistent with the high recombination constant and low injection regime. In this context is interesting to estimate de concentrations of electrons available in the device according to Eq. (2):

$$n_s = \frac{k_B T L}{q^2 A R_w D_{eff}} \tag{2}$$

Where k_B is the Boltzmann constant, T is the absolute temperature, q is the fundamental charge and A is the active surface. n_s is estimated to be 1.17×10^{16} cm^{-3}, this value is comparatively low with other devices and it is consistent with the high value of diffusion coefficient and recombination constant ratio. This behavior can be ascribed to a poor charge injection from the NS-GQD to the NaNT even though the global electrical resistance is lowered probably due to microstructural features induced by the interaction between NaNT and NS-GQD. Complementarily, the transport dynamics were studied in terms of IMVS and IMPS spectroscopies, as depicted in Fig. 7.

For this purpose, the device is illuminated under a modulated white LED light which drives to a generation of excess carriers according to the continuity equation [36], without considering the possibility of trapping and detrapping and modified considering a polychromatic light according to Eq. (3).

$$\frac{d\delta n}{dt} = \eta \int \alpha(\lambda) I_0 e^{-\alpha(\lambda)x} d\lambda + D_n \frac{d^2(\delta n)}{dt^2} - \frac{\delta n}{\tau} \tag{3}$$

where δn represents the excess carrier concentration, η represents the efficiency of carrier photogeneration factor and α the absorptivity of the system, Dn is the diffusion coefficient and τ is the recombination time. The QDSSC was illuminated under three different illumination intensities and the recombination (τ_{rec}) and transport (τ_{trans}) time were obtained from the fitting of the imaginary part of the characteristic signal vs the frequency [29]. The obtained characteristics times and the estimated charge collection efficiency (η_{cc}) and diffusion coefficients (D_{eff}) are summarized in Table 3.

The results obtained by these techniques are consistent with those obtained by impedance spectroscopy analysis. The high recombination times and diffusion coefficient are consistent with a high charge collec-

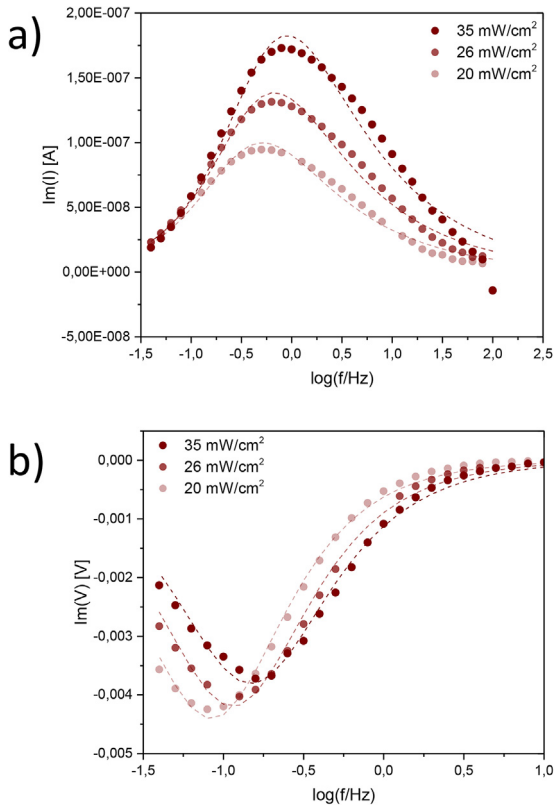

Fig. 7. Imaginary part of the a) IMPS and b) IMVS spectrum (circles) and their fitting function (dashed lines) for the QDSSC.

tion efficiency subrogated to the low charge injection levels. No dramatic differences are seen when varying the illumination intensity.

Taking into account all the previous characterization, the main advantageous properties of these composites are the interesting enhancement of the electronic transport properties compared to the pristine sodium titanate nanotubes. For these reasons we consider that these materials could also be explored for electron transport properties in perovskites solar cells [37,38].

4. Conclusions

We report the successful synthesis of $Na_2Ti_2O_5{\cdot}H_2O$ decorated with N,S co-doped graphene quantum dots. The distinctive features were evidenced for the heterostructures by means of transmission electron microscopy, Raman spectroscopy and X-ray diffraction studies. It can be concluded that N,S co-doped graphene quantum dots intercalations in the interlaminar space of the titanate leads to a certain degree of unwrapping of the nanotubes as particularly suggested by our Raman spectroscopy and X-ray diffraction studies. Our nanoscale heterostructures yielded to an order of magnitude enhancement in the electric conductivity interpreted in terms of favorable interactions between the NS-GQD and the NaNT acting as proper connectors. Finally, our QDSSC solar cell prototype yielded a relatively low cell parameters but with an efficient charge collection mechanism (0.74) and long recombination times (~ 1 s). These systems could be further explored for electron transport layer applications for perovskites solar cells in order to take advantage of the improvements in electron transport.

Declaration of Competing Interest

The authors declare that they have no known competing financial interests or personal relationships that could have appeared to influence the work reported in this paper.

Data Availability

Data will be made available on request.

acknowledgement

The authors wish to thank Uruguayan funding institutions: CSIC, ANII (Fondo María Viñas), CAP and PEDECIBA.

References

[1] L. Yang, D. Yin, Y. Shen, M. Yang, X. Li, X. Han, X. Jiang, B. Zhao, Mesoporous semiconducting TiO 2 with rich active sites as a remarkable substrate for surface-enhanced Raman scattering, Phys. Chem. Chem. Phys. 19 (2017) 18731–18738.
[2] R. Faccio, L. Fernández-Werner, H. Pardo, A.W. Mombru, Current trends in materials for dye sensitized solar cells, Recent Pat. Nanotechnol. 5 (2011) 46–61.
[3] R. Jose, V. Thavasi, S. Ramakrishna, Metal oxides for dye-sensitized solar cells, J. Am. Ceram. Soc. 92 (2009) 289–301.
[4] C.C. Raj, R. Prasanth, A critical review of recent developments in nanomaterials for photoelectrodes in dye sensitized solar cells, J. Power Sources 317 (2016) 120–132.
[5] J. Yang, S. Mei, J. Ferreira, Hydrothermal synthesis of TiO2 nanopowders from tetraalkylammonium hydroxide peptized sols, Mater. Sci. Eng. C 15 (2001) 183–185.
[6] T. Sugimoto, X. Zhou, A. Muramatsu, Synthesis of uniform anatase TiO2 nanoparticles by gel–sol method: 4. Shape control, J. Colloid Interface Sci. 259 (2003) 53–61.
[7] M. Wang, J. Bai, F.Le Formal, S.-J. Moon, L. Cevey-Ha, R. Humphry-Baker, C. Grätzel, S.M. Zakeeruddin, M. Grätzel, Solid-state dye-sensitized solar cells using ordered TiO2 nanorods on transparent conductive oxide as photoanodes, J. Phys. Chem. C 116 (2012) 3266–3273.
[8] D.V. Bavykin, V.N. Parmon, A.A. Lapkin, F.C. Walsh, The effect of hydrothermal conditions on the mesoporous structure of TiO 2 nanotubes, J. Mater. Chem. 14 (2004) 3370–3377.
[9] B.C. Viana, O.P. Ferreira, A.G. Souza Filho, A.A. Hidalgo, J. Mendes Filho, O.L. Alves, Alkali metal intercalated titanate nanotubes: a vibrational spectroscopy study, Vib. Spectrosc. 55 (2011) 183–187.
[10] X. Hou, K. Aitola, P.D. Lund, TiO2 nanotubes for dye-sensitized solar cells—a review, Energy Sci. Eng. 9 (2021) 921–937.
[11] A. Salant, M. Shalom, I. Hod, A. Faust, A. Zaban, U. Banin, Quantum dot sensitized solar cells with improved efficiency prepared using electrophoretic deposition, ACS Nano 4 (2010) 5962–5968.
[12] B. Li, L. Wang, B. Kang, P. Wang, Y. Qiu, Review of recent progress in solid-state dye-sensitized solar cells, Sol. Energy Mater. Sol. Cells 90 (2006) 549–573.
[13] R. Senthamarai, V. Madurai Ramakrishnan, B. Palanisamy, S. Kulandhaivel, Synthesis of TiO2 nanostructures by green approach as photoanodes for dye-sensitized solar cells, Int. J. Energy Res. 45 (2021) 3089–3096.
[14] L. Kang, Y. Guo, P. Miao, M. Sun, B. Song, P. Xu, X. Liu, Study of surface plasmon assisted reactions to understand the light-induced decarboxylation of N719 sensitizer, Eur. J. Inorg. Chem. 2019 (2019) 23–28.
[15] J.D. Roy-Mayhew, I.A. Aksay, Graphene materials and their use in dye-sensitized solar cells, Chem. Rev. 114 (2014) 6323–6348.
[16] T. Jiang, L. Zhang, M. Ji, Q. Wang, Q. Zhao, X. Fu, H. Yin, Carbon nanotubes/TiO2 nanotubes composite photocatalysts for efficient degradation of methyl orange dye, Particuology 11 (2013) 737–742.
[17] J. Ji, L.L. Zhang, H. Ji, Y. Li, X. Zhao, X. Bai, X. Fan, F. Zhang, R.S. Ruoff, Nanoporous Ni (OH) 2 thin film on 3D ultrathin-graphite foam for asymmetric supercapacitor, ACS Nano 7 (2013) 6237–6243.
[18] H. Tian, K. Shen, X. Hu, L. Qiao, W. Zheng, N, S co-doped graphene quantum dots-graphene-TiO2 nanotubes composite with enhanced photocatalytic activity, J. Alloys Compd. 691 (2017) 369–377.
[19] S. Chinnusamy, R. Kaur, A. Bokare, F. Erogbogbo, Incorporation of graphene quantum dots to enhance photocatalytic properties of anatase TiO2, MRS Commun. 8 (2018) 137–144.
[20] S. Kundu, P. Sarojinijeeva, R. Karthick, G. Anantharaj, G. Saritha, R. Bera, S. Anandan, A. Patra, P. Ragupathy, M. Selvaraj, Enhancing the efficiency of DSSCs by the modification of TiO2 photoanodes using N, F and S, co-doped graphene quantum dots, Electrochim. Acta 242 (2017) 337–343.
[21] S.P. Lim, A. Pandikumar, H.N. Lim, R. Ramaraj, N.M. Huang, Boosting photovoltaic performance of dye-sensitized solar cells using silver nanoparticle-decorated N, S–Co-doped-TiO2 photoanode, Sci. Rep. 5 (2015) 1–14.
[22] T. Kasuga, M. Hiramatsu, A. Hoson, T. Sekino, K. Niihara, Formation of titanium oxide nanotube, Langmuir 14 (1998) 3160–3163.
[23] M. Esteves, L. Fernández-Werner, F. Pignanelli, M. Romero, M.R. Chialanza, R. Faccio, Á.W. Mombrú, A step forward towards the structural characterization of Na2Ti2O5· H2O nanotubes and their correlation with optical and electric transport properties, Ceram. Int. 46 (2020) 2877–2886.
[24] D. Qu, M. Zheng, P. Du, Y. Zhou, L. Zhang, D. Li, H. Tan, Z. Zhao, Z. Xie, Z. Sun, Highly luminescent S, N co-doped graphene quantum dots with broad visible absorption bands for visible light photocatalysts, Nanoscale 5 (2013) 12272–12277.
[25] M.A. Aegerter, M. Mennig, Sol-gel Technologies For Glass Producers and Users, Springer Science & Business Media, 2013.
[26] M. Esteves, L. Fernández-Werner, F. Pignanelli, B. Montenegro, M. Belluzzi, M. Pistón, M.R. Chialanza, R. Faccio, Á.W. Mombrú, Synthesis, characterization and simulation of lithium titanate nanotubes for dye sensitized solar cells, Ceram. Int. 45 (2019) 708–717.

[27] M. Esteves, D. Mombrú, M. Romero, L. Fernández-Werner, R. Faccio, A.W. Mombrú, Insights on the structural and electrical transport of sodium titanate nanotubes decorated with CuInS2 quantum dots heterostructures, Appl. Surf. Sci. 535 (2021) 147733.
[28] D. Mombrú, M. Romero, R. Faccio, Á.W. Mombrú, Tuning electrical transport mechanism of polyaniline–graphene oxide quantum dots nanocomposites for potential electronic device applications, J. Phys. Chem. C 120 (2016) 25117–25123.
[29] S. Kim, D. Hee Shin, C. Oh Kim, S. Seok Kang, S. Sin Joo, S.-.H. Choi, S. Won Hwang, C. Sone, Size-dependence of Raman scattering from graphene quantum dots: interplay between shape and thickness, Appl. Phys. Lett. 102 (2013) 053108.
[30] D. Porezag, M.R. Pederson, Infrared intensities and Raman-scattering activities within density-functional theory, Phys. Rev. B 54 (1996) 7830.
[31] J. Mistrik, S. Kasap, H.E. Ruda, C. Koughia, J. Singh, Optical properties of electronic materials: fundamentals and characterization, Springer Handbook of Electronic and Photonic Materials, Springer, 2017 1-1.
[32] T. Gao, H. Fjellvåg, P. Norby, Crystal structures of titanate nanotubes: a Raman scattering study, Inorg. Chem. 48 (2009) 1423–1432.
[33] L. Yang, B. Kruse, Revised Kubelka–Munk theory. I. Theory and application, JOSA A 21 (2004) 1933–1941.
[34] M. Adachi, M. Sakamoto, J. Jiu, Y. Ogata, S. Isoda, Determination of parameters of electron transport in dye-sensitized solar cells using electrochemical impedance spectroscopy, J. Phys. Chem. B 110 (2006) 13872–13880.
[35] T. Oekermann, D. Zhang, T. Yoshida, H. Minoura, Electron transport and back reaction in nanocrystalline TiO2 films prepared by hydrothermal crystallization, J. Phys. Chem. B 108 (2004) 2227–2235.
[36] L. Peter, K. Wijayantha, Intensity dependence of the electron diffusion length in dye-sensitised nanocrystalline TiO2 photovoltaic cells, Electrochem. Commun. 1 (1999) 576–580.
[37] S. Zheng, G. Wang, T. Liu, L. Lou, S. Xiao, S. Yang, Materials and structures for the electron transport layer of efficient and stable perovskite solar cells, Sci. China Chem. 62 (2019) 800–809.
[38] M.F.M. Noh, C.H. Teh, R. Daik, E.L. Lim, C.C. Yap, M.A. Ibrahim, N.A. Ludin, A.R. bin Mohd Yusoff, J. Jang, M.A.M. Teridi, The architecture of the electron transport layer for a perovskite solar cell, J. Mater. Chem. C 6 (2018) 682–712.